**THE EUROPEAN
PHYSICAL JOURNAL C**

Reheating constraints on modified single-field natural inflation models

Hua Zhou[1,2,a], **Qing Yu**[1,2,b], **Yu Pan**[3,c], **Ruiyu Zhou**[3,d], **Wei Cheng**[3,e]

[1] Department of Physics, Chongqing Key Laboratory for Strongly Coupled Physics, Chongqing University, Chongqing 401331, People's Republic of China
[2] Department of Physics, Norwegian University of Science and Technology, Høgskoleringen 5, 7491 Trondheim, Norway
[3] School of Science, Chongqing University of Posts and Telecommunications, Chongqing 400065, People's Republic of China

Abstract In this paper, we discuss three modified single-field natural inflation models in detail, including Special generalized natural inflation model (SNI), extended natural inflation model (ENI) and natural inflation inspired model (NII). We derive the analytical expression of the tensor-to-scalar ratio r and the spectral index n_s for those models. Then the reheating temperature T_{re} and reheating duration N_{re} are analytically derived. Moreover, considering the CMB constraints, the feasible space of the SNI model in (n_s, r) plane is almost covered by that of the NII, which means the NII is more general than the SNI. In addition, there is no overlapping space between the ENI and the other two models in (n_s, r) plane, which indicates that the ENI and the other two models exclude each other, and more accurate experiments can verify them. Furthermore, the reheating brings tighter constraints to the inflation models, but they still work for a different reheating universe. Considering the constraints of n_s, r, N_k and choosing T_{re} near the electroweak energy scale, one can find that the decay constants of the three models have no overlapping area and the effective equations of state ω_{re} should be within $\frac{1}{4} \lesssim \omega_{re} \lesssim \frac{4}{5}$ for the three models.

1 Introduction

The inflation theory is one of the accepted solutions to the problem of horizon and flatness in Big Bang cosmology [1–7]. The quantum fluctuations of the inflaton field provide a piece of fundamental knowledge for studying the anisotropy of the cosmic microwave background (CMB) [8–13] and the structure of the universe [14–17]. At present, the predictions of scale-invariant inflation, Gaussian and adiabatic density perturbations have been confirmed by WMAP [18], COBE [19], Planck [20] and so on.

The single scalar field inflation model that relies on the slow-rolling is now the mainstream inflation model [21–27], which is described by its potential $V(\phi)$. When the slope and curvature of $V(\phi)$ are small enough to satisfy the slow-roll conditions, the universe will continue to inflate. At the end of inflation, the universe goes into the next period which is usually called reheating [28]. During the reheating, the energy density in the inflaton is transformed into a thermal bath, which fills the universe at the beginning of the era of radiation dominance. The reheating scenarios have a complex physics, where the duration of the reheating would be affected by the speed and type of particles, and there is usually a so-called preheating stage. In this stage, the inflation field decays into massive particles through non-perturbative processes such as parametric resonance and instantaneous preheating [29–32]. After the preheating, the frequency band with parametric resonance will have very high occupancy, while the rest of space will be in a highly non-thermal state [33].

The reheating stage can be parameterized with the reheating temperature T_{re}, the effective equation of state(eos) ω_{re} of the matter in the reheating process, and the reheating duration, i.e., number of e-foldings N_{re}. For the value of T_{re}, it should be larger than the electroweak scale to meet the requirement of producing weak-scale dark matter. In addition, to reach the temperature of big bang nucleosynthesis, T_{re} should be greater than 10 MeV [34,35]. Furthermore, considering the constraints of the late entropy produced by the decay of massive particles, the T_{re} would be as low as [2.5–4] MeV [34,35].

[a] e-mail: zhouhua@cqu.edu.cn

[b] e-mail: yuq@cqu.edu.cn

[c] e-mail: panyu@cqupt.edu.cn

[d] e-mail: zhoury@cqupt.edu.cn

[e] e-mail: chengwei@cqupt.edu.cn (corresponding author)

Reheating is an extremely complex physical process [36], and it is difficult for us to directly detect and study. Typically, to avoid the complexity of reheating and simplify the description, the default choice of EOS ω_{re} is the constant in the interval $[-1/3, 1]$ [33,37–39], where $\omega_{re} = -1/3$ corresponds to the end of inflation, and in order to satisfy the dominant energy condition of general relativity and maintain causality, ω_{re} must be less than 1 [39–41]. However, the EOS ω_{re} should vary with time during the reheating stage due to the non-equilibrium nonlinear dynamics of the field [37,42]. Therefore, Ref. [42] discusses the time evolution equation of EOS during this stage and obtain a time-varying EOS equation, which alleviates the arbitrariness of defining EOS parameters during reheating. To this end, we will take the average ω_{re} during reheating for subsequent discussion based on the analysis of the evolution equation of EOS between the coherent oscillation and the radiation-dominated period in Ref. [42], and give more details in Sect. 4.2.

Furthermore, the number of e-folding N_k from the end of inflation to the start of the radiation era is usually chosen to define the duration of reheating. The value of e-foldings N_k is affected by the potential of inflation, the universe reheating instantaneously affects the upper limit of e-folding numbers, and the reheating temperature under the electroweak scale determines the lower limit. The value of N_k can be between 46 and 70 to deal with the horizon problem [44], and according to the analysis in Refs. [45,46], N_k can even be 107 in some extreme cases.

The natural inflation (NI) model was first proposed in Ref. [47]. It has been a research hotspot in this field for several years because of its simple and clear formula, and it also produced the mass of pseudo-Goldstone bosons through non-perturbation effects. Moreover, the NI model has the shift symmetry, which can prevent the influence of radiative correction on potential [48]. Unfortunately, due to the limitation of the tensor-to-scalar ratio r, recent Planck + BICEP/Keck observations have ruled out the NI model [20,49]. Since then, a large number of modified NI models have appeared [50–59], in this paper, we will study the three modified single-filed NI models and consider the constraints of CMB and reheating for three models.

The main contents of this article are as follows: in Sect. 2, we will review the method of parameterization of reheating and derive the expressions of the reheating temperature T_{re} and reheating duration N_{re}. In Sect. 3, we derive r, n_s, and reheating parameters for three modified single-field NI models. In Sect. 4, we will explore the CMB and reheating constraints on those models and discuss their feasible intervals to satisfy the experimental conditions. In Sect. 5, is reserved for a summary.

2 Reheating

After inflation is over, the energy of the universe exists in the scalar field. At this point, the temperature of the universe drops, and nucleosynthesis is pushed beyond the trigger boundary. Reheating is a transitional stage after the end of the inflation, which can release the energy in the scalar field and heat the universe, thereby ensuring the smooth appearance of the radiation-dominated period. As mentioned before, the reheating phase can be parameterized as temperature T_{re}, effective state equation ω_{re} and duration e-folding number N_{re}.

Next, we will give the derivations of T_{re} and N_{re} in detail from inflation models [38,60,61]. According to the energy density evolution equation in the inflation universe, we can get $\rho \propto \alpha^{-3(1+\omega)}$, and

$$\frac{\rho_{end}}{\rho_{re}} = \left(\frac{a_{end}}{a_{re}}\right)^{-3(1+\omega_{re})}, \tag{1}$$

where "*end*" and "*re*" represent the end of inflation and reheating, respectively. From Eq. 1, the e-folding number of reheating can be expressed as

$$N_{re} = \frac{1}{3(1+\omega_{re})} \ln\left(\frac{\rho_{end}}{\rho_{re}}\right), \tag{2}$$

furthermore, $\omega_{re} = -\frac{1}{3}$ corresponds to the end of inflation, and one can get $\rho_{end} = \frac{3}{2}V_{end}$. After reheating, the universe will enter a period of radiation dominance and the energy density has the relationship with the reheating temperature $\rho_{re} = \frac{1}{30}\pi^2 g_{re} T_{re}^4$. Where g_{re} is dominant for the number of relativistic species at the end of reheating, and we use $g_{re} \approx 100$ for the following discussion in this article. Therefore, the duration N_{re} can be further expressed as a function of T_{re}

$$N_{re} = \frac{1}{3(1+\omega_{re})} \ln\left(\frac{45 V_{end}}{\pi^2 g_{re} T_{re}^4}\right). \tag{3}$$

Considering the variation of the number of helical states in the radiant gas as a function of temperature [33], the relationship between the reheating temperature T_{re} and todays temperature T_0 is obtained as

$$\begin{aligned} T_{re} &= T_0\left(\frac{a_0}{a_{re}}\right)\left(\frac{43}{11g_{re}}\right)^{\frac{1}{3}} \\ &= T_0\left(\frac{a_0}{a_{eq}}\right)e^{N_{RD}}\left(\frac{43}{11g_{re}}\right)^{\frac{1}{3}}, \end{aligned} \tag{4}$$

where the subscripts "*eq*" and "*RD*" represent the matter-dominated period and radiation-dominated epoch, respectively. And $e^{N_{RD}} = \frac{a_{eq}}{a_{re}}$ with the length in e-folds of radiation dominance N_{RD}. The time to cross the Hubble radius during inflation is represented by pivot scale $k = a_k H_k$ including a Hubble parameter during the inflation H_k, thus we can rewrite

the ratio a_0/a_{eq} into

$$\frac{a_0}{a_{eq}} = \frac{a_0 H_k}{k} e^{-N_k} e^{-N_{re}} e^{-N_{RD}}, \tag{5}$$

where $e^{N_k} = a_{end}/a_k$ and $e^{N_{re}} = a_{re}/a_{end}$, and "$k''$" denotes the value of Fourier mode k when it leaves the Hubble radius during inflation. Then Eq. 4 can be rewritten as

$$T_{re} = \left(\frac{43}{11 g_{re}}\right)^{\frac{1}{3}} \left(\frac{a_0 T_0}{k}\right) H_k e^{-N_k} e^{-N_{re}}. \tag{6}$$

Two special cases need to be considered, e.g., $\omega_{re} = \frac{1}{3}$ and $\omega_{re} \neq \frac{1}{3}$. First, assuming $\omega_{re} \neq \frac{1}{3}$ and putting Eq. 6 into Eq. 3, one can get

$$N_{re} = \frac{4}{1 - 3\omega_{re}} \left[-\frac{1}{4} \ln\left(\frac{45}{\pi^2 g_{re}}\right) - \ln\left(\frac{V_{end}^{\frac{1}{4}}}{H_k}\right) \right.$$
$$\left. -\frac{1}{3} \ln\left(\frac{11 g_{re}}{43}\right) - \ln\left(\frac{k}{a_0 T_0}\right) - N_k \right]. \tag{7}$$

If we choose the Planck pivot $0.05 \, \mathrm{Mpc}^{-1}$, the Eq. 7 simplifies to

$$N_{re} = \frac{4}{1 - 3\omega_{re}} \left[61.6 - \ln\left(\frac{V_{end}^{\frac{1}{4}}}{H_k}\right) - N_k \right]. \tag{8}$$

Likewise, Eq. 6 can also be abbreviated as

$$T_{re} = \left[\left(\frac{43}{11 g_{re}}\right)^{\frac{1}{3}} \frac{a_0 T_0}{k} H_k e^{-N_k} \right.$$
$$\left. \times \left(\frac{45 V_{end}}{\pi^2 g_{re}}\right)^{-\frac{1}{3(1+\omega_{re})}} \right]^{\frac{3(1+\omega_{re})}{3\omega_{re}-1}}. \tag{9}$$

In the second case, e.g., $\omega_{re} = \frac{1}{3}$, Eq. 3 becomes

$$0 = \frac{1}{4} \ln\left(\frac{30}{\pi^2 g_{re}}\right) + \frac{1}{4} \ln\left(\frac{3}{2}\right) + \ln\left(\frac{V_{end}^{\frac{1}{4}}}{H_k}\right)$$
$$+ \frac{1}{3} \ln\left(\frac{11 g_{re}}{43}\right)$$
$$+ \ln\left(\frac{k}{a_0 T_0}\right) + N_k, \tag{10}$$

and if one chooses $g_{re} = 100$, then the above formula can be simplified to

$$61.55 = \ln\left(\frac{V_{end}^{\frac{1}{4}}}{H_k}\right) + N_k. \tag{11}$$

Since $\omega_{re} = \frac{1}{3}$ corresponds to the start of the radiation-dominated period, it's impossible to obtain the expressions for N_{re} and T_{re}, but we can obtain the constraints on n_s for a particular model.

3 Inflaton potentials

The theoretical motivation for the NI model is clear and simple in form, but it is contradicted by observational data with more than 95% confidence, especially with the recently published experimental data of Planck + BICEP/Keck [20,49]. Based on this, many studies on modification of the NI model have been reported [50–59], which is expected to match the experimental data. This paper focuses on three modified single-field NI models, we derive the tensor-to-scalar ratio r and spectral index n_s of the models, and investigate the reheating constraints on these models.

3.1 Special generalized natural inflation

According to the generalized natural inflation [50],

$$V(\phi) = \Lambda^4 \left[\cos\frac{\phi}{f_m} + \varepsilon \cos\frac{\phi}{f_m} + e^{\frac{1}{n_1!} \cos\left(\frac{\phi}{f_m} + \frac{\pi}{n_1!}\right)^{n_1}} \right]^{n_2}, \tag{12}$$

a special generalized natural inflation (SNI) model can be obtained with $n_1 = \pm\infty$, $n_2 = 1$ and $\varepsilon = 0$, where Λ^4 represents the energy density and f_m is the decay constant.

The e-folds number N_k is defined as

$$N_k = \frac{1}{M_p^2} \int_{\phi_{end}}^{\phi_k} \frac{V}{V'} d\phi, \tag{13}$$

where the subscript "end''" refers to the value of the inflation field at the end of inflation. According to the definition of slow-roll parameters $\epsilon = \frac{M_p^2}{2}\left(\frac{V'}{V}\right)^2$ and $\eta = M_p^2 \frac{V''}{V}$, choosing $\epsilon = 1$ as the end of inflation, we can derive

$$\phi_{end} = \frac{1}{f_m} \arccos\left(\sqrt{\frac{M_p^2}{2f_m^2 + M_p^2}}\right). \tag{14}$$

By using the spectral index $n_s = 1 - 6\epsilon + 2\eta$ and $r = 16\epsilon$ at $\phi = \phi_k$, this will lead to

$$n_s = \frac{f_m^2 - M_p^2 \left[3\tan^2\left(\frac{\phi_k}{f_m}\right) + 2 \right]}{f_m^2}, \tag{15}$$

and

$$r = -\frac{8[f_m^2(n_s - 1) + 2M_p^2]}{3f_m^2}. \tag{16}$$

According to $H_k = \pi M_p \sqrt{8 A_s \epsilon}$ and $V \approx 3 H_k^2 M_p^2$, the Hubble parameter H_k can be directly deduced as

$$H_k = \frac{2\sqrt{3}\pi M_p \sqrt{-A_s[f_m^2(n_s - 1) + 2M_p^2]}}{3 f_m}, \tag{17}$$

and the potential of the end of the inflation V_{end} becomes

$$V_{end} = 4\pi^2 A_s M_p^4 \left(-2\frac{M_p^2}{f_m^2} - n_s + 1\right) \frac{\cos\left(\frac{\phi_{end}}{f_m}\right)}{\cos\left(\frac{\phi_k}{f_m}\right)}, \quad (18)$$

where the expression of $\phi_k(n_s)$ can be obtained by inversely solving Eq. 15, the scalar amplitude $A_s \approx 2.196 \times 10^{-9}$ and $M_p = 2.4 \times 10^{18}$ GeV [62].

3.2 Extended Natural Inflation model

The second model, we can call it the "Extended" natural inflation (ENI) model. Where the inflaton is the pseudo-Nambo–Goldstone boson and the shift symmetry preserves the flatness of the potential, it can be written as [39]

$$V(\phi) = \frac{2\Lambda^4}{2^m}\left(1 + \cos\frac{\phi}{f_e}\right)^m, \quad (19)$$

where f_e is the decay constant for the ENI model, and the application scope of the model can be expanded by changing the value of the parameter m. Following the method in the previous section, the r, n_s, H_k and V_{end} of the ENI model can be obtained as follows:

$$r = -8m\frac{f_e^2(n_s - 1) + mM_p^2}{f_e^2(m + 1)}, \quad (20)$$

$$n_s = 1 - \frac{mM_p^2 \sec^2\left(\frac{\phi_k}{2f_e}\right)\left[m\cos\left(\frac{\phi_k}{f_e}\right) - m - 2\right]}{2f_e^2}, \quad (21)$$

$$H_k = 2\pi M_p \sqrt{-A_s \frac{m[f_e^2(n_s - 1) + mM_p^2]}{f_e^2(m + 1)}}, \quad (22)$$

and

$$V_{end} = -12\pi^2 A_s m^2 M_p^4 \frac{[m^2 M_p^2 - f_e^2(n_s - 1)]}{f_e^2(m + 1)^2}$$
$$\times \frac{[f_e^2(n_s - 1) + mM_p^2]}{(2f_e^2 + m^2 M_p^2)}. \quad (23)$$

3.3 Natural inflation inspired model

The third model is the natural inflation inspired (NII) model, which is able to make the spontaneous symmetry breaking scale less than 1 [63] and its potential can be expressed as

$$V(\phi) = V_0\left[1 - \sin^2\left(\frac{\phi}{f_n}\right)\right], \quad (24)$$

where f_n is the decay parameter for the NII model and one can do the same steps as the SNI model, it is obtained

$$n_s = 1 - 2\frac{M_p^2}{f_n^2}\left[\cos\left(\frac{2\phi_k}{f_n}\right) - 3\right]\sec^2\left(\frac{\phi_k}{f_n}\right), \quad (25)$$

$$r = 16\epsilon = -\frac{2[f_n^2(n_s - 1) + 4M_p^2]^2}{f_n^4(n_s - 1)}, \quad (26)$$

$$H_k = \sqrt{2}\pi M_p \sqrt{A_s\left(-\frac{4M_p^2}{f_n^2} - n_s + 1\right)}, \quad (27)$$

and

$$V_{end} = -\frac{3\pi^2 A_s M_p^4[4M_p^2 - f_n^2(n_s - 1)][4M_p^2 + f_n^2(n_s - 1)]}{2f_n^2(f_n^2 + 2M_p^2)}. \quad (28)$$

4 Results

4.1 CMB constraints

Figure 1 shows the relationship between n_s and r under different N_k for SNI, ENI, and NII. For each model, we take two different e-folding numbers, which $N_k = 55$ and $N_k = 65$ correspond to up and down lines, respectively. The Gradient graph indicates the value of decay constant varying from $1M_p$ to $30M_p$. The light blue and light grey shaded broadband stand for the latest experiments with 1σ and 2σ experiment errors of BAO, BICEP/KECK, and Planck data, respectively [49].
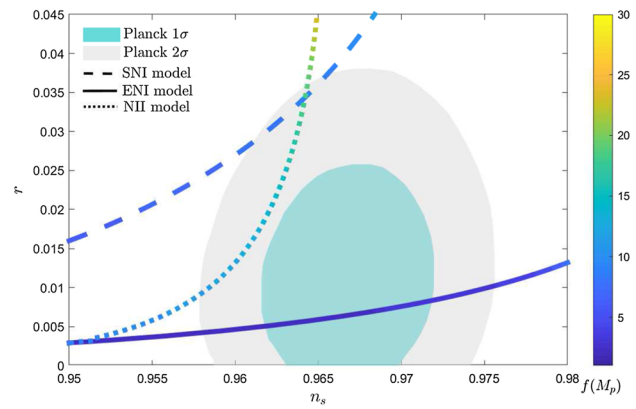
In Fig. 1, the dashed line represents the feasible parameter space of n_s and r of the SNI model and $N_k \in [55, 65]$. In the SNI model, the r value matches the experimental data within 2σ error when $N_k \geq 55$, and the value of r matches the experimental data within 1σ error when $N_k \geq 65$. Furthermore, with the constrained by CMB, the decay constants are in the range of $8M_p$–$10M_p$. The solid line represents the feasible parameter space of the ENI model and we will choose $m = 0.1$ for the following discussion. In the ENI model, the parameter spaces of r and n_s are consistent with the latest experimental data with 1σ error when N_k varies in [55–65] and the decay constant is constrained to be less than $2M_p$. The r and n_s of the NII model dependence curves under different e-folds numbers are shown as dotted lines of Fig. 1. When $N_k \geq 55$, the obtained results are within the error of the 2σ experimental data. In addition, when $N_k > 60$, r can falls within the experimental boundary of 1σ Planck data. Moreover, the CMB constrained decay constant is in the range of $12M_p$–$20M_p$.

Figure 1 graphically shows that the NII model is more general than the SNI model since the feasible space of the
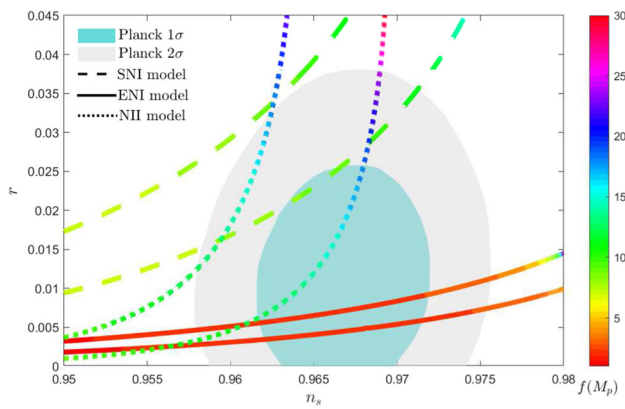
Fig. 1 The relationship between r and n_s for three single-field NI models under different $N_k \in [55, 65]$. The dashed line, solid and dotted lines represent the relationship between $n_s - r$ under the SNI model, ENI model, and NII model, respectively. Among the ENI model, we choose $m = 0.1$ for subsequent discussion. The colored gradient graph corresponds to the value of decay constant varying from $1M_p$ to $30M_p$. In addition, the light blue and light grey broadband correspond to the latest combination 1σ and 2σ experiment errors of BAO, BICEP/KECK, and Planck data, respectively [49]

Fig. 2 The relationship between r and n_s for three single-field NI models under the special case $\omega_{re} = \frac{1}{3}$ and the constraints of the amplitude of scalar fluctuations. The dashed line, solid and dotted lines represent the relationship between $n_s - r$ under the SNI model, ENI model, and NII model, respectively. The colored gradient graph corresponds to the value of decay constant varying from $1M_p$ to $30M_p$. In addition, the light blue and light grey broadband correspond to the latest combination 1σ and 2σ experiment errors of BAO, BICEP/KECK, and Planck data, respectively [49]

SNI model on the (n_s, r) plane is almost covered by NII under the constraints of the CMB. In addition, there's no overlapping part in the space of (n_s, r) between the ENI model and the other two models, which indicates the ENI model is excluded by the other two models, and we need more accurate experiments to confirm it.

When the values of $H_k = \pi M_p \sqrt{8A_s\epsilon}$, N_k and V_{end} for the three models are brought into

$$\ln\left(\frac{V_{end}^{\frac{1}{4}}}{H_k}\right) + N_k - 61.55, \tag{29}$$

then we can get the (n_s, r) for $\omega_{re} = \frac{1}{3}$ and constraints of the amplitude of scalar fluctuations A_s, as shown in the Fig. 2. Where the dashed line, solid and dotted lines represent the relationship between $n_s - r$ under the SNI model, ENI model, and NII model, respectively. Likewise, the colored gradient graph indicates the decay constant varies from $1M_p$ to $30M_p$. The above conditions impose strong constraints on the parameter space. For the SNI model, only when the decay constant $8M_p < f_m < 10M_p$, n_s and r would be within the 2σ experiment boundary.

It can be seen from Fig. 2 that for any chosen value of f_e under the ENI model, the r can satisfy the constraints given by the latest experiments, however, n_s is very sensitive to the change of parameter f_e. Under the constraints of the amplitude of scalar fluctuations, n_s of the ENI model would be within experimental error when $f_e \rightarrow 2M_p$ and varies in a small range [49]. In addition, when $f_e > 4M_p$, the r and n_s of the ENI model tend to be stable and change in a small range.

Under the constraint of amplitude of scalar fluctuations, the variation of r and n_s with f_n is shown in Fig. 2. Where the the dotted line represents the change curve of the NII model. As Fig. 2 shows, those above conditions impose strong constraints on the parameter space. Only when $f_n \in [14M_p, 20M_p]$, n_s and r can be within the range of the latest 2σ Planck experiment [49], far from the experimental range of 1σ.

4.2 Reheating constraints

The value of EOS can be fixed by the inflation model parameter p when the scalar field oscillates near the minimum potential at the end of inflation, i.e. the EOS of a homogeneous condensate oscillating in potential with a minimum of the form $V(\phi) \propto \phi^p$ can be parameterized as $\omega = (p - 2)/(p + 2)$, and this allows us to naturally derive the value of EOS at this stage [37,40,42,43,64]. However, at the end of the coherent oscillation phase, fragmentation leads to inhomogeneities, which in turn alter the EOS during the phase of backreaction [42,65–69]. The effects of fragmentation on the evolution equation of EOS at this stage can usually be obtained through lattice simulation, see [43,67,69,70] for more details. Furthermore, the Ref. [42] studies the EOS in the reheating phase after coherent oscillation in detail, and gives a more precise EOS for this stage.

Based on this, as an attempt, we also analyze the minimum potential behavior of the three models listed in this paper. However, we found that there is a constant correction term in the expanded form of the three models, and the effect of this correction may require lattice calculations to estimate,
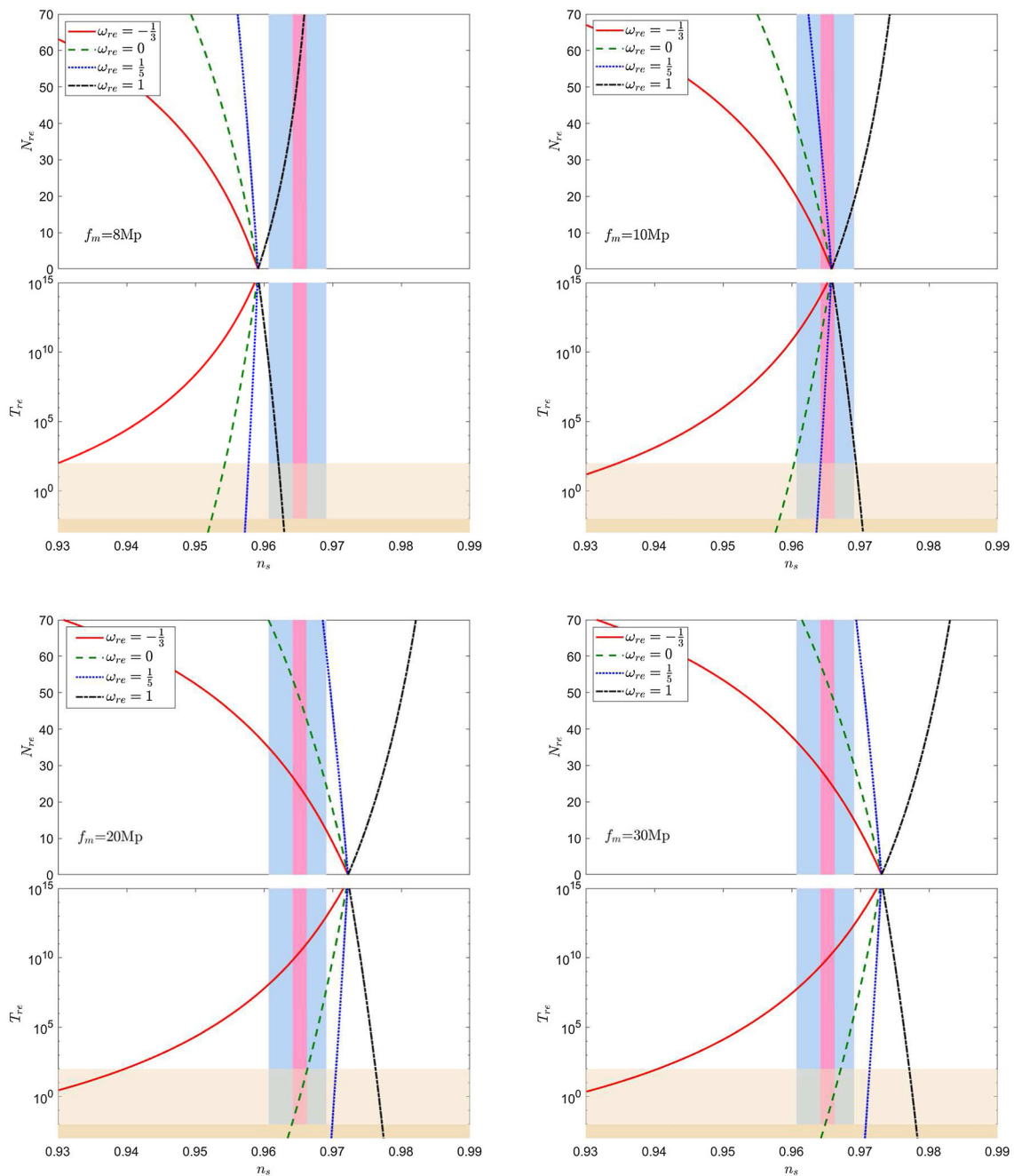
Fig. 3 T_{re} and N_{re} as a function of n_s for different f_m and ω_{re} in the SNI model. The red solid, the gree dashed, the blue dotted and the black dotted and dashed line corresponds to $\omega_{re} = -\frac{1}{3}$, $\omega_{re} = 0$, $\omega_{re} = \frac{1}{5}$ and $\omega_{re} = 1$, respectively. The blue region corresponds to the 1σ boundary of Planck n_s and the red area corresponds to the 1σ boundary of the further CMB experiment with sensitivity $\pm 10^{-3}$ [72,73]. The khaki area corresponds to temperatures of 10 MeV from BBN, and Light khaki areas correspond to electroweak scales below 100 GeV

which is very challenging work. Fortunately, the value of EOS has a manageable impact on subsequent research in this paper. Therefore, assuming that the constant coefficient correction is small enough and we can infer the $V(\phi) \propto \phi^2$ near the minimum potential for the three models. Then, the EOS at different stages can be obtained naturally based on

Ref. [42], i.e. $\omega_{re} = -\frac{1}{3}$, $\omega_{re} = 0$, $\omega_{re} = \frac{1}{5}$ and $\omega_{re} = 1$, where $\omega_{re} = 0$ stands for the coherent oscillation stage and $\omega_{re} = 1/5$ for the reheating stage.

The behaviors of N_{re} and T_{re} as a function of n_s under the SNI model as shown in Fig. 3, the blue region corresponds to the 1σ boundary on Planck's n_s and the red one corresponds
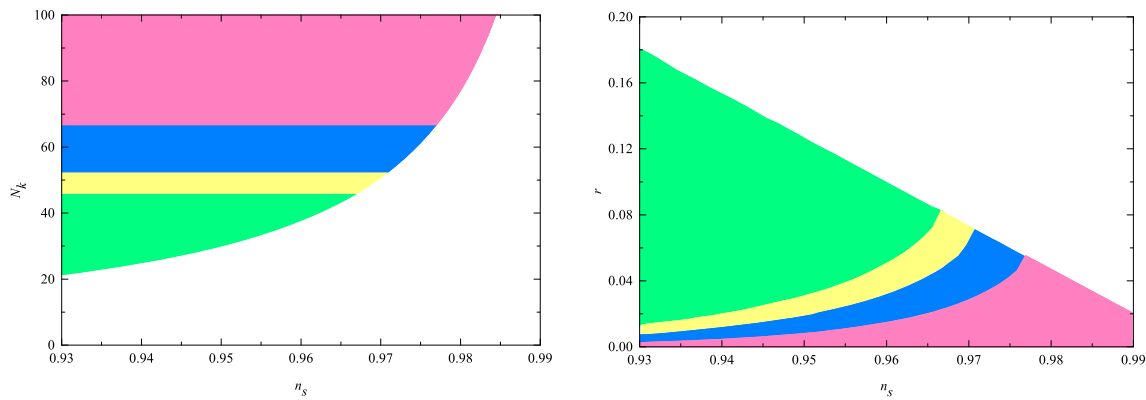
Fig. 4 The N_k vs n_s and r vs n_s under the SNI model, where $f_m < 30M_p$. The green area corresponds to $\omega_{re} \leq 0$, the yellow area corresponds to $0 \leq \omega_{re} \leq \frac{1}{5}$, the blue area represents the range of $\frac{1}{5} \leq \omega_{re} \leq 1$, and $\omega_{re} \geq 1$ corresponds to the dark pink range

Table 1 The values of n_s, N_k and r under the SNI model corresponds to different values of f_m and ω_{re}, where $T_{re} = 100$ GeV

$f_m(M_p)$	ω_{re}	n_s	N_k	r
8	$[-\frac{1}{3}, 0]$	[0.9300, 0.9543]	[25.12, 46.04]	[0.1033, 0.0385]
	$[0, \frac{1}{5}]$	[0.9543, 0.9578]	[46.04, 52.93]	[0.0385, 0.0293]
	$[\frac{1}{5}, \frac{1}{3}]$	[0.9578, 0.9591]	[52.93, 56.37]	[0.0293, 0.0257]
	$[\frac{1}{3}, 1]$	[0.9591, 0.9621]	[56.37, 66.62]	[0.0257, 0.0176]
10	$[-\frac{1}{3}, 0]$	[0.9347, 0.9604]	[25.16, 46.13]	[0.1208, 0.0524]
	$[0, \frac{1}{5}]$	[0.9604, 0.9642]	[46.13, 53.04]	[0.0524, 0.0420]
	$[\frac{1}{5}, \frac{1}{3}]$	[0.9642, 0.9658]	[53.04, 56.49]	[0.0420, 0.0379]
	$[\frac{1}{3}, 1]$	[0.9658, 0.9694]	[56.49, 66.80]	[0.0379, 0.0283]
20	$[-\frac{1}{3}, 0]$	[0.9397, 0.9663]	[25.20, 46.24]	[0.1474, 0.0764]
	$[0, \frac{1}{5}]$	[0.9663, 0.9705]	[46.24, 53.19]	[0.0764, 0.0653]
	$[\frac{1}{5}, \frac{1}{3}]$	[0.9705, 0.9722]	[53.19, 56.66]	[0.0653, 0.0608]
	$[\frac{1}{3}, 1]$	[0.9722, 0.9762]	[56.66, 67.03]	[0.0608, 0.0500]
30	$[-\frac{1}{3}, 0]$	[0.9397, 0.9672]	[25.21, 46.26]	[0.1548, 0.0816]
	$[0, \frac{1}{5}]$	[0.9672, 0.9714]	[46.26, 53.22]	[0.0816, 0.0705]
	$[\frac{1}{5}, \frac{1}{3}]$	[0.9714, 0.9731]	[53.22, 56.69]	[0.0705, 0.0659]
	$[\frac{1}{3}, 1]$	[0.9731, 0.9771]	[56.69, 67.07]	[0.0659, 0.0551]

to the further experiment precision of 10^{-3}. According to the constraints of CMB on the model parameter space, we choose four typical values of f_m for subsequent discussion, i.e., $f_m = 8M_p$, $f_m = 10M_p$, $f_m = 20M_p$ and $f_m = 30M_p$. The T_{re} converges around 10^{15} GeV, which may be required by the GUT-scale regeneration model [71]. The point where the four lines come together ($N_{re} = 0$) is what be called the instantaneous reheating point [44].

The relationship between $N_k - n_s$ and $r - n_s$ is obvious in Fig. 4. The green area corresponds to $\omega_{re} \leq 0$, the yellow area corresponds to $0 \leq \omega_{re} \leq \frac{1}{5}$, the blue area represents the range of $\frac{1}{5} \leq \omega_{re} \leq 1$, and $\omega_{re} \geq 1$ corresponds to the dark pink range. Since the value of f_m is proportional to n_s, the lower bound of the $N_k - n_s$ corresponds to larger f_m-values, conversely, the upper bound of the $r - n_s$ corresponds to larger f_m. One can also find that, both r and n_s are within the

Planck-2018 constraint when $\omega_{re} > 0$. If one sets $T_{re} = 100$ GeV, thus the bounds of n_s, N_k and r all can be obtained from the constraints with different f_m and ω_{re}. From Table 1 one can get that ω_{re} is proportional to n_s and N_k, and inversely proportional to r. Furthermore, under such restriction of T_{re}, the corresponding ω_{re} can be found only when $f_m < 10M_p$, one can find the solution that both n_s and r are within the latest Planck-2018 data [49].

Figure 5 shows N_{re} and T_{re} as a function of n_s under the ENI model. By varying the decay constants f_e in the feasible interval, e.g., $2M_p$, $4M_p$, $10M_p$ and $30M_p$, one can find that the ENI model is sensitive to the choice of parameter when $f_e < 4M_p$, i.e., $f_e > 2M_p$, the central value is rapidly away from the experimental error range and tends to be stable after $f_e > 4M_p$. Under four different f_e, the value of n_s, r and N_k for different ω_{re} can be found in Table 2. when $f_e \geq 4M_p$
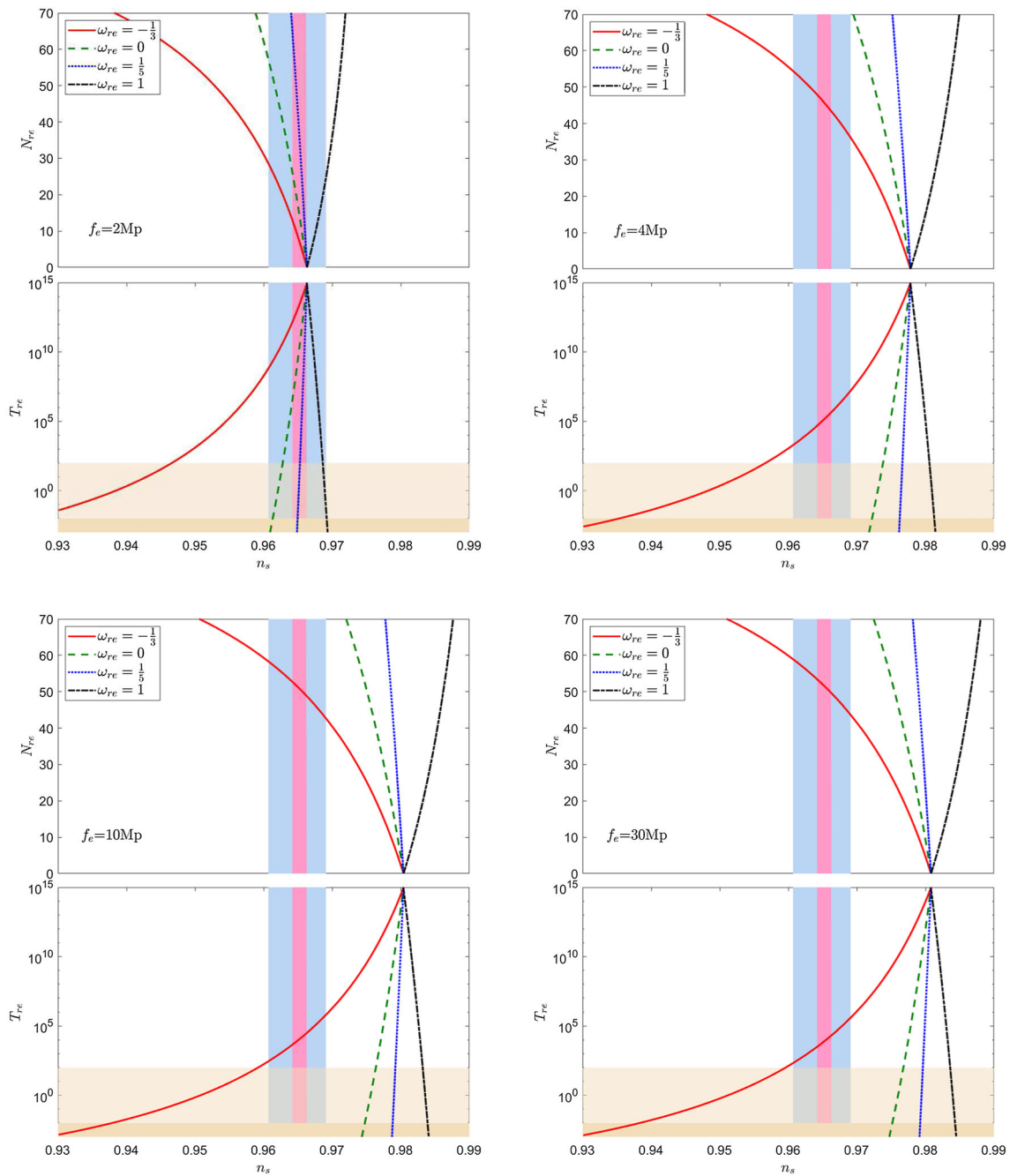
Fig. 5 The duration of reheating N_{re} and the temperature T_{re} as a function of n_s are plotted for different parameters f_e and ω_{re} of the ENI model. The legend of the shadow area refer to Fig. 3

and $0 \leq \omega_{re} \leq 1$, n_s is totally excluded by the Planck-2018. While, the value of r satisfy the experimental constraints [49] for any chosen of $f_e < 30M_p$ and $\omega_{re} \in [-1/3, 1]$. Figure 6 shows the relationship between the predictions of $N_k - n_s$ and $r - n_s$ for different ω_{re}, and one can find that when $\omega_{re} > 0$, the value of r can within the experimental error.

The change of the temperature T_{re} and the duration of reheating N_{re} with n_s under the NII model is shown in Fig. 7. Four typical f_n have been chosen, i.e., $f_n = 10M_p$,

$f_n = 15M_p$, $f_n = 20M_p$, and $f_n = 30M_p$, and one can find when $f_n > 20M_p$, the predictions of N_{re} and T_{re} tend to be stable. Table 3. further show the variation of n_s vs r and N_k vs r under different effective equation of state ω_{re}. It can be seen that when $f_n = 10M_p$, the value of r can fall within the experimentally allowable boundaries when $0 < \omega_{re} < 1$. However, even if a larger ω_{re} is chosen, the value of n_s is still smaller than the experimental value. Fortunately, when $15M_p \leq f_n \leq 20M_p$, both n_s and r can within Planck-

Table 2 The values of n_s, N_k and r under the ENI model corresponding to different f_e and ω_{re}, where $T_{re} = 100$ GeV

$f_e(M_p)$	ω_{re}	n_s	N_k	r
2	$[-\frac{1}{3}, 0]$	[0.9466, 0.9628]	[27.05, 47.14]	[0.0206, 0.0089]
	$[0, \frac{1}{5}]$	[0.9628, 0.9653]	[47.14, 53.74]	[0.0089, 0.0070]
	$[\frac{1}{5}, \frac{1}{3}]$	[0.9653, 0.9663]	[53.74, 57.03]	[0.0070, 0.0063]
	$[\frac{1}{3}, 1]$	[0.9663, 0.9686]	[57.03, 66.86]	[0.0063, 0.0046]
4	$[-\frac{1}{3}, 0]$	[0.9567, 0.9738]	[27.17, 47.35]	[0.0270, 0.0145]
	$[0, \frac{1}{5}]$	[0.9738, 0.9766]	[47.35, 53.99]	[0.0145, 0.0124]
	$[\frac{1}{5}, \frac{1}{3}]$	[0.9766, 0.9778]	[53.99, 57.30]	[0.0124, 0.0116]
	$[\frac{1}{3}, 1]$	[0.9778, 0.9806]	[57.30, 67.19]	[0.0116, 0.0096]
10	$[-\frac{1}{3}, 0]$	[0.9592, 0.9764]	[27.20, 47.41]	[0.0290, 0.0165]
	$[0, \frac{1}{5}]$	[0.9764, 0.9792]	[47.41, 54.06]	[0.0165, 0.0144]
	$[\frac{1}{5}, \frac{1}{3}]$	[0.9792, 0.9804]	[54.06, 57.37]	[0.0144, 0.0135]
	$[\frac{1}{3}, 1]$	[0.9804, 0.9832]	[57.37, 67.28]	[0.0135, 0.0115]
30	$[-\frac{1}{3}, 0]$	[0.9596, 0.9768]	[27.21, 47.42]	[0.0293, 0.0168]
	$[0, \frac{1}{5}]$	[0.9768, 0.9796]	[47.42, 54.07]	[0.0168, 0.0147]
	$[\frac{1}{5}, \frac{1}{3}]$	[0.9796, 0.9808]	[54.07, 57.39]	[0.0147, 0.0139]
	$[\frac{1}{3}, 1]$	[0.9808, 0.9836]	[57.39, 67.29]	[0.0139, 0.0118]
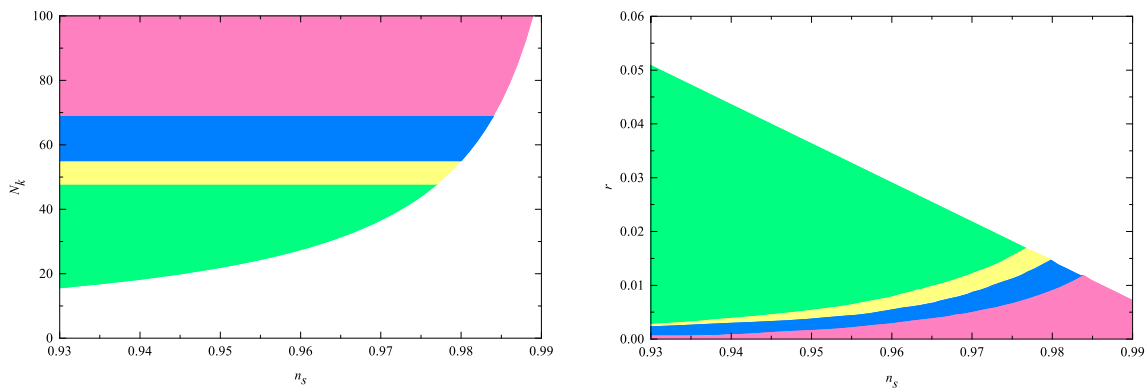
Fig. 6 N_k vs n_s and r vs n_s under the ENI model, where $f_e < 30M_p$. The legend of the shadow area refer to Fig. 4

2018 error range under the constraints of $\frac{1}{5} \leq \omega_{re} \leq 1$ [49]. When $f_n > 30M_p$, the values of r is outside the experimental error range under any choice of ω_{re}. In Fig. 8, it is graphically shows the changes of N_k vs n_s and r vs n_s under the constraints of ω_{re}, especially when $0 \leq \omega_{re} \leq \frac{1}{5}$, one can find the n_s and r lie within the contour constrained by Planck-2018.

Combining the constraints of CMB and reheating, Fig. 9 shows the value of the effective state equations ω_{re} of reheating for SNI, ENI, and NII models at different values of decay constants. Where the red solid line, the blue dashed line, and the black dotted line correspond to the SNI, ENI, and NII models, respectively. One can find that the decay constants of the three models are mutually exclusive. Furthermore, for the SNI model, the n_s, r and N_k all satisfy the constraints of the Planck-2018 when the eos $0.27 < \omega_{re} < 0.86$. For the ENI and NII models, in order to satisfy the constraints of the

n_s, r and N_k, ω_{re} should be within $0.24 < \omega_{re} < 0.84$ and $0.36 < \omega_{re} < 0.80$, respectively.

5 Summary

Reheating is an important period of inflation theory, which can release the energy stored in the scalar field at the end of inflation and increase the temperature of the universe. In this work, we study the evolution of the reheating after the end of inflation and investigate the constraints of the CMB and reheating for different single-filed natural inflation models. The variation trends of reheating temperature N_{re} and duration T_{re} with ω_{re} and n_s were explored.

The CMB constraints show that the n_s and r feasible space obtained by the SNI model is almost covered by the NII model, which means that the NII model is more general than
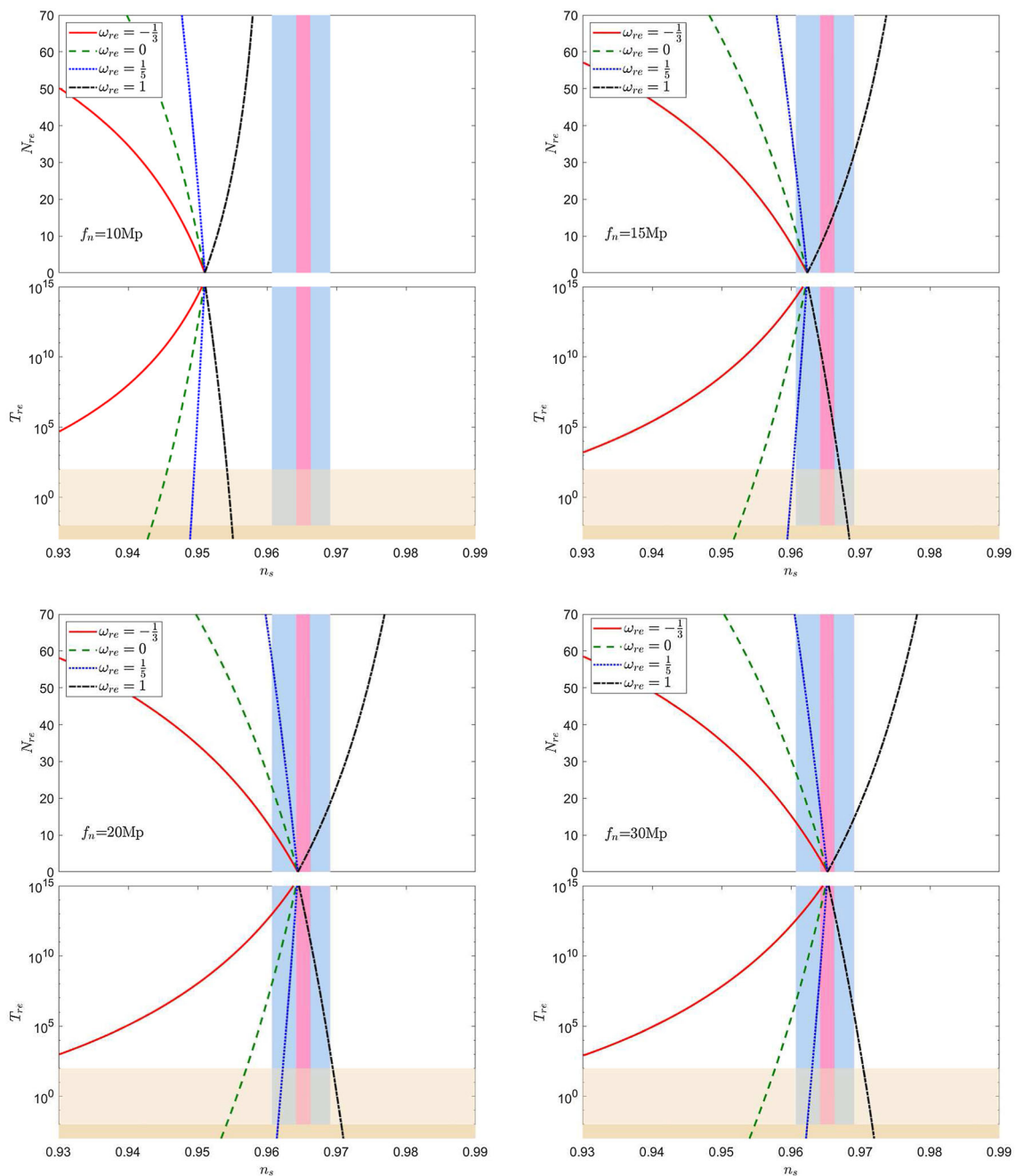
Fig. 7 T_{re} and N_{re} as a function of n_s for different f_n and ω_{re} in the NII model. The legend of the shadow area refer to Fig. 3

the SNI model. Furthermore, the ENI model has no overlapping area with the other two models, which indicates that the ENI model and the other two models exclude each other, and more accurate experiments can separate them.

Considering the constraint of reheating, we find that the reheating equation of state ω_{re} can effectively narrow the feasible parameter space of the model, and greatly increase the accuracy of the model. Moreover, we restrict ω_{re} to the range $-\frac{1}{3} \leq \omega_{re} \leq 1$, resulting in tighter constraints on the

parameters of the inflation model than from the usual procedure. To this end, we explore the constraints of CMB and reheating for three modified single-filed natural inflation models and the results show that the decay constants are different for the three models, moreover, the effective equations of state ω_{re} should fall in the interval $\frac{1}{4} \lesssim \omega_{re} \lesssim \frac{4}{5}$ for three models.

Table 3 The values of n_s, N_k and r under different f_n and ω_{re} of the NII model, where $T_{re} = 100$ GeV

$f_n(M_p)$	ω_{re}	n_s	N_k	r
10	$[-\frac{1}{3}, 0]$	[0.9171, 0.9457]	[25.81, 46.60]	[0.0444, 0.0076]
	$[0, \frac{1}{5}]$	[0.9457, 0.9495]	[46.60, 53.42]	[0.0076, 0.0043]
	$[\frac{1}{5}, \frac{1}{3}]$	[0.9495, 0.9510]	[53.42, 56.82]	[0.0043, 0.0033]
	$[\frac{1}{3}, 1]$	[0.9510, 0.9542]	[56.82, 66.96]	[0.0033, 0.0015]
15	$[-\frac{1}{3}, 0]$	[0.9230, 0.9553]	[25.94, 46.84]	[0.0912, 0.0325]
	$[0, \frac{1}{5}]$	[0.9553, 0.9603]	[46.84, 53.71]	[0.0325, 0.0242]
	$[\frac{1}{5}, \frac{1}{3}]$	[0.9603, 0.9623]	[53.71, 57.13]	[0.0242, 0.0210]
	$[\frac{1}{3}, 1]$	[0.9623, 0.9670]	[57.13, 67.37]	[0.0210, 0.0140]
20	$[-\frac{1}{3}, 0]$	[0.9240, 0.9570]	[25.98, 46.92]	[0.1146, 0.0506]
	$[0, \frac{1}{5}]$	[0.9570, 0.9623]	[46.92, 53.81]	[0.0506, 0.0408]
	$[\frac{1}{5}, \frac{1}{3}]$	[0.9623, 0.9644]	[53.81, 57.24]	[0.0408, 0.0368]
	$[\frac{1}{3}, 1]$	[0.9644, 0.9695]	[57.24, 67.51]	[0.0368, 0.0276]
30	$[-\frac{1}{3}, 0]$	[0.9245, 0.9577]	[26.02, 46.99]	[0.1338, 0.0677]
	$[0, \frac{1}{5}]$	[0.9577, 0.9630]	[46.99, 53.89]	[0.0677, 0.0572]
	$[\frac{1}{5}, \frac{1}{3}]$	[0.9630, 0.9652]	[53.89, 57.32]	[0.0572, 0.0529]
	$[\frac{1}{3}, 1]$	[0.9652, 0.9704]	[57.32, 67.60]	[0.0529, 0.0427]
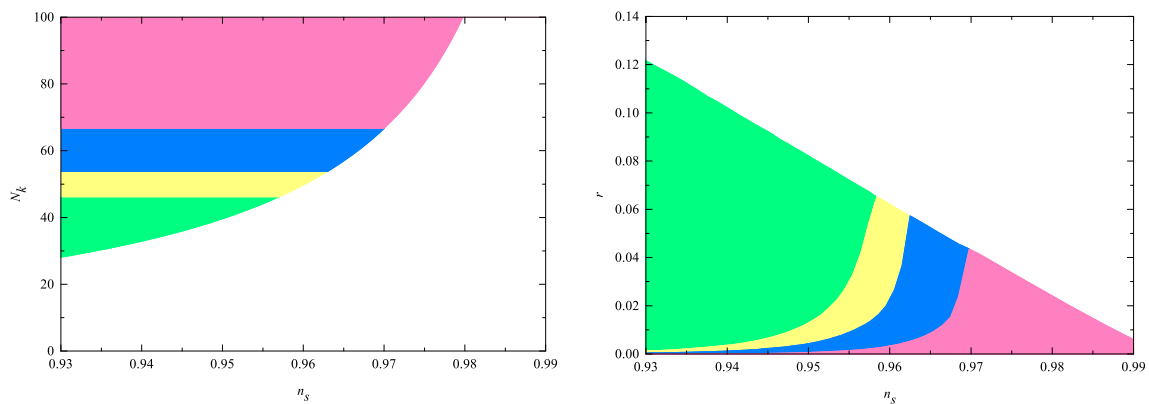
Fig. 8 N_k vs n_s and r vs n_s under NII model, where $f_n < 30M_p$. The legend of the shadow area refer to Fig. 4
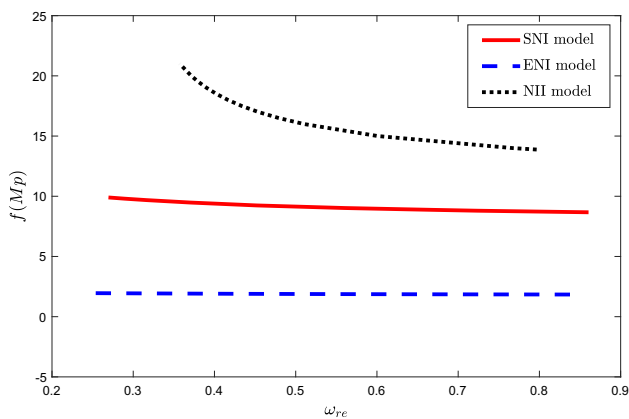
Fig. 9 Feasible parameter space comparison of SNI, ENI, and NII models under CMB and reheating constraints

Data Availability Statement This manuscript has no associated data or the data will not be deposited. [Authors' comment: All the figures and the numerical predictions can be derived from the formulas presented in the paper, so the data do not need to be deposited].

References

1. A.A. Starobinsky, A new type of isotropic cosmological models without singularity. Phys. Lett. B **91**, 99–102 (1980). https://doi.org/10.1016/0370-2693(80)90670-X
2. D. Baumann, Inflation. https://doi.org/10.1142/9789814327183_0010. arXiv:0907.5424 [hep-th]
3. W.H. Kinney, Cosmology, inflation, and the physics of nothing. NATO Sci. Ser. **II**(123), 189–243 (2003). https://doi.org/10.1007/978-94-010-0076-5_5
4. A.H. Guth, The inflationary universe: a possible solution to the horizon and flatness problems. Phys. Rev. D **23**, 347–356 (1981). https://doi.org/10.1103/PhysRevD.23.347
5. K. Sato, First order phase transition of a vacuum and expansion of the universe. Mon. Not. R. Astron. Soc. **195**, 467–479 (1981). https://doi.org/10.1093/mnras/195.3.467
6. A. Albrecht, P.J. Steinhardt, Cosmology for grand unified theories with radiatively induced symmetry breaking. Phys. Rev. Lett. **48**, 1220–1223 (1982). https://doi.org/10.1103/PhysRevLett.48.1220
7. A.D. Linde, A new inflationary universe scenario: a possible solution of the horizon, flatness, homogeneity, isotropy and primordial monopole problems. Phys. Lett. B **108**, 389–393 (1982). https://doi.org/10.1016/0370-2693(82)91219-9
8. E.W. Kolb, M.S. Turner, The early universe. Front. Phys. **69**, 1–547 (1990). https://doi.org/10.1201/9780429492860
9. D.H. Lyth, A. Riotto, Particle physics models of inflation and the cosmological density perturbation. Phys. Rep. **314**, 1–146 (1999). https://doi.org/10.1016/S0370-1573(98)00128-8
10. C. Armendariz-Picon, T. Damour, V.F. Mukhanov, k-inflation. Phys. Lett. B **458**, 209–218 (1999). https://doi.org/10.1016/S0370-2693(99)00603-6
11. V.F. Mukhanov, H.A. Feldman, R.H. Brandenberger, Theory of cosmological perturbations. Part 1. Classical perturbations. Part 2. Quantum theory of perturbations. Part 3. Extensions. Phys. Rep. **215**, 203–333 (1992). https://doi.org/10.1016/0370-1573(92)90044-Z
12. A. De Felice, S. Tsujikawa, f(R) theories. Living Rev. Relaiv. **13**, 3 (2010). https://doi.org/10.12942/lrr-2010-3
13. W. Cheng, Y. He, J.W. Diao, Y. Pan, J. Zeng, J.W. Zhang, A new way to test the WIMP dark matter models. JHEP **08**, 124 (2021). https://doi.org/10.1007/JHEP08(2021)124
14. A.H. Guth, S.Y. Pi, Fluctuations in the new inflationary universe. Phys. Rev. Lett. **49**, 1110–1113 (1982). https://doi.org/10.1103/PhysRevLett.49.1110
15. A.H. Guth, S.Y. Pi, The quantum mechanics of the scalar field in the new inflationary universe. Phys. Rev. D **32**, 1899–1920 (1985). https://doi.org/10.1103/PhysRevD.32.1899
16. A.A. Starobinsky, Dynamics of phase transition in the new inflationary universe scenario and generation of perturbations. Phys. Lett. B **117**, 175–178 (1982). https://doi.org/10.1016/0370-2693(82)90541-X
17. V.F. Mukhanov, G.V. Chibisov, Quantum fluctuations and a nonsingular universe. JETP Lett. **33**, 532–535 (1981). https://inspirehep.net/literature/170051
18. E. Komatsu et al., [WMAP], Seven-Year Wilkinson Microwave Anisotropy Probe (WMAP) Observations: Cosmological Interpretation. Astrophys. J. Suppl. **192**, 18 (2011). https://doi.org/10.1088/0067-0049/192/2/18
19. G.F. Smoot, C.L. Bennett, A. Kogut et al., Structure in the COBE differential microwave radiometer first-year maps. Astrophys. J. Suppl. **396**, L1–L5 (1992). https://doi.org/10.1086/186504
20. Y. Akrami et al. [Planck], Planck 2018 results. X. Constraints on inflation. Astron. Astrophys. **641**, A10 (2020). https://doi.org/10.1051/0004-6361/201833887
21. P. Creminelli, D. LópezNacir, M. Simonović, G. Trevisan, M. Zaldarriaga, ϕ^2 or Not ϕ^2: testing the simplest inflationary potential. Phys. Rev. Lett. **112**, 241303 (2014). https://doi.org/10.1103/PhysRevLett.112.241303
22. N. Kaloper, L. Sorbo, A natural framework for chaotic inflation. Phys. Rev. Lett. **102**, 121301 (2009). https://doi.org/10.1103/PhysRevLett.102.121301
23. I. Dalianis, G.P. Kodaxis, I.D. Stamou, N. Tetradis, A. Tsigkas-Kouvelis, Spectrum oscillations from features in the potential of single-field inflation. Phys. Rev. D **104**, 103510 (2021). https://doi.org/10.1103/PhysRevD.104.103510
24. D.A. Steer, F. Vernizzi, Tachyon inflation: tests and comparison with single scalar field inflation. Phys. Rev. D **70**, 043527 (2004). https://doi.org/10.1103/PhysRevD.70.043527
25. G. Geshnizjani, R. Brandenberger, Back reaction of perturbations in two scalar field inflationary models. JCAP **04**, 006 (2005). https://doi.org/10.1088/1475-7516/2005/04/006
26. X. Chen, R. Easther, E.A. Lim, Large non-Gaussianities in single field inflation. JCAP **06**, 023 (2007). https://doi.org/10.1088/1475-7516/2007/06/023
27. D. Seery, J.E. Lidsey, Primordial non-Gaussianities in single field inflation. JCAP **06**, 003 (2005). https://doi.org/10.1088/1475-7516/2005/06/003
28. R. Allahverdi, R. Brandenberger, F.Y. Cyr-Racine, A. Mazumdar, Reheating in inflationary cosmology: theory and applications. Ann. Rev. Nucl. Part. Sci. **60**, 27–51 (2010). https://doi.org/10.1146/annurev.nucl.012809.104511
29. L. Kofman, A.D. Linde, A.A. Starobinsky, Reheating after inflation. Phys. Rev. Lett. **73**, 3195–3198 (1994). https://doi.org/10.1103/PhysRevLett.73.3195
30. L. Kofman, A.D. Linde, A.A. Starobinsky, Towards the theory of reheating after inflation. Phys. Rev. D **56**, 3258–3295 (1997). https://doi.org/10.1103/PhysRevD.56.3258
31. G.N. Felder, L. Kofman, A.D. Linde, Instant preheating. Phys. Rev. D **59**, 123523 (1999). https://doi.org/10.1103/PhysRevD.59.123523
32. J.F. Dufaux, G.N. Felder, L. Kofman, M. Peloso, D. Podolsky, Preheating with trilinear interactions: tachyonic resonance. JCAP **07**, 006 (2006). https://doi.org/10.1088/1475-7516/2006/07/006
33. J.L. Cook, E. Dimastrogiovanni, D.A. Easson, L.M. Krauss, Reheating predictions in single field inflation. JCAP **04**, 047 (2015). https://doi.org/10.1088/1475-7516/2015/04/047
34. M. Kawasaki, K. Kohri, N. Sugiyama, Cosmological constraints on late time entropy production. Phys. Rev. Lett. **82**, 4168 (1999). https://doi.org/10.1103/PhysRevLett.82.4168
35. M. Kawasaki, K. Kohri, N. Sugiyama, MeV scale reheating temperature and thermalization of neutrino background. Phys. Rev. D **62**, 023506 (2000). https://doi.org/10.1103/PhysRevD.62.023506
36. S.Y. Khlebnikov, I.I. Tkachev, The universe after inflation: the wide resonance case. Phys. Lett. B **390**, 80–86 (1997). https://doi.org/10.1016/S0370-2693(96)01419-0

37. D.I. Podolsky, G.N. Felder, L. Kofman, M. Peloso, Equation of state and beginning of thermalization after preheating. Phys. Rev. D **73**, 023501 (2006). https://doi.org/10.1103/PhysRevD.73.023501

38. L. Dai, M. Kamionkowski, J. Wang, Reheating constraints to inflationary models. Phys. Rev. Lett. **113**, 041302 (2014). https://doi.org/10.1103/PhysRevLett.113.041302

39. J.B. Munoz, M. Kamionkowski, Equation-of-state parameter for reheating. Phys. Rev. D **91**(4), 043521 (2015). https://doi.org/10.1103/PhysRevD.91.043521

40. S.S. Mishra, V. Sahni, A.A. Starobinsky, Curing inflationary degeneracies using reheating predictions and relic gravitational waves. JCAP **05**, 075 (2021). https://doi.org/10.1088/1475-7516/2021/05/075

41. P.H. Chavanis, Cosmology with a stiff matter era. Phys. Rev. D **92**(10), 103004 (2015). https://doi.org/10.1103/PhysRevD.92.103004

42. P. Saha, S. Anand, L. Sriramkumar, Accounting for the time evolution of the equation of state parameter during reheating. Phys. Rev. D **102**(10), 103511 (2020). https://doi.org/10.1103/PhysRevD.102.103511

43. K.D. Lozanov, M.A. Amin, Self-resonance after inflation: oscillons, transients and radiation domination. Phys. Rev. D **97**(2), 023533 (2018). https://doi.org/10.1103/PhysRevD.97.023533

44. P. Pareek, A. Nautiyal, Reheating constraints on k-inflation. Phys. Rev. D **104**, 083526 (2021). https://doi.org/10.1103/PhysRevD.104.083526

45. S. Dodelson, L. Hui, A horizon ratio bound for inflationary fluctuations. Phys. Rev. Lett. **91**, 131301 (2003). https://doi.org/10.1103/PhysRevLett.91.131301

46. A.R. Liddle, S.M. Leach, How long before the end of inflation were observable perturbations produced? Phys. Rev. D **68**, 103503 (2003). https://doi.org/10.1103/PhysRevD.68.103503

47. K. Freese, J.A. Frieman, A.V. Olinto, Natural inflation with pseudo-Nambu–Goldstone bosons. Phys. Rev. Lett. **65**, 3233–3236 (1990). https://doi.org/10.1103/PhysRevLett.65.3233

48. F.C. Adams, J.R. Bond, K. Freese, J.A. Frieman, A.V. Olinto, Natural inflation: particle physics models, power law spectra for large scale structure, and constraints from COBE. Phys. Rev. D **47**, 426–455 (1993). https://doi.org/10.1103/PhysRevD.47.426

49. P.A.R. Ade et al., [BICEP and Keck], Improved constraints on primordial gravitational waves using Planck, WMAP, and BICEP/Keck observations through the 2018 observing season. Phys. Rev. Lett. **127**, 151301 (2021). https://doi.org/10.1103/PhysRevLett.127.151301

50. W. Cheng, L. Bian, Y.F. Zhou, Axionlike particle inflation and dark matter. Phys. Rev. D **104**, 063010 (2021). https://doi.org/10.1103/PhysRevD.104.063029

51. W. Cheng, T. Qian, Q. Yu, H. Zhou, R.Y. Zhou, Gravitational wave from axionlike particle inflation. Phys. Rev. D **104**, 103502 (2021). https://doi.org/10.1103/PhysRevD.104.103502

52. I. Antoniadis, A. Karam, A. Lykkas, T. Pappas, K. Tamvakis, Rescuing quartic and natural inflation in the Palatini formalism. JCAP **03**, 005 (2019). https://doi.org/10.1088/1475-7516/2019/03/005

53. Y. Nomura, T. Watari, M. Yamazaki, Pure natural inflation. Phys. Lett. B **776**, 227–230 (2018). https://doi.org/10.1016/j.physletb.2017.11.052

54. J.P. Hong, M. Kawasaki, M. Yamazaki, Oscillons from pure natural inflation. Phys. Rev. D **98**, 043531 (2018). https://doi.org/10.1103/PhysRevD.98.043531

55. R.Z. Ferreira, A. Notari, G. Simeon, Natural inflation with a periodic non-minimal coupling. JCAP **11**, 021 (2018). https://doi.org/10.1088/1475-7516/2018/11/021

56. G. Simeon, Scalar–tensor extension of natural inflation. JCAP **07**, 028 (2020). https://doi.org/10.1088/1475-7516/2020/07/028

57. Y. Reyimuaji, X. Zhang, Natural inflation with a nonminimal coupling to gravity. JCAP **03**, 059 (2021). https://doi.org/10.1088/1475-7516/2021/03/059

58. A. Salvio, Natural-scalaron inflation. JCAP **10**, 011 (2021). https://doi.org/10.1088/1475-7516/2021/10/011

59. X. Zhang, C.Y. Chen, Y. Reyimuaji, Modified gravity models for inflation: in conformity with observations. Phys. Rev. D **105**, 043514 (2022). https://doi.org/10.1103/PhysRevD.105.043514

60. R. Easther, H.V. Peiris, Bayesian analysis of inflation II: model selection and constraints on reheating. Phys. Rev. D **85**, 103533 (2012). https://doi.org/10.1103/PhysRevD.85.103533

61. J. Mielczarek, Reheating temperature from the CMB. Phys. Rev. D **83**, 023502 (2011). https://doi.org/10.1103/PhysRevD.83.023502

62. P.A.R. Ade et al. [Planck], Planck 2015 results. XX. Constraints on inflation. Astron. Astrophys. **594**, A20 (2016). https://doi.org/10.1051/0004-6361/201525898

63. G. German, A Natural Inflation inspired model, Gen. Rel. Grav. **54**, 48 (2022). https://doi.org/10.1007/s10714-022-02935-2

64. M.S. Turner, Coherent scalar field oscillations in an expanding universe. Phys. Rev. D **28**, 1243 (1983). https://doi.org/10.1103/PhysRevD.28.1243

65. R. Micha, I.I. Tkachev, Relativistic turbulence: a long way from preheating to equilibrium. Phys. Rev. Lett. **90**, 121301 (2003). https://doi.org/10.1103/PhysRevLett.90.121301

66. R. Micha, I.I. Tkachev, Turbulent thermalization. Phys. Rev. D **70**, 043538 (2004). https://doi.org/10.1103/PhysRevD.70.043538

67. M.A. Amin, R. Easther, H. Finkel, Inflaton fragmentation and oscillon formation in three dimensions. JCAP **12**, 001 (2010). https://doi.org/10.1088/1475-7516/2010/12/001

68. M.A. Amin, M.P. Hertzberg, D.I. Kaiser, J. Karouby, Nonperturbative dynamics of reheating after inflation: a review. Int. J. Mod. Phys. D **24**, 1530003 (2014). https://doi.org/10.1142/S0218271815300037

69. D. Maity, P. Saha, (P)reheating after minimal plateau inflation and constraints from CMB. JCAP **07**, 018 (2019). https://doi.org/10.1088/1475-7516/2019/07/018

70. K.D. Lozanov, M.A. Amin, Equation of state and duration to radiation domination after inflation. Phys. Rev. Lett. **119**, 061301 (2017). https://doi.org/10.1103/PhysRevLett.119.061301

71. K.E. Bourakadi, M. Bousder, Z. Sakhi, M. Bennai, Preheating and reheating constraints in supersymmetric braneworld inflation. Eur. Phys. J. Plus **136**, 888 (2021). https://doi.org/10.1140/epjp/s13360-021-01887-x

72. L. Amendola et al. [Euclid Theory Working Group], Cosmology and fundamental physics with the Euclid satellite. Living Rev. Relativ. **16**, 6 (2013). https://doi.org/10.1007/s41114-017-0010-3

73. P. Andre et al. [PRISM], PRISM (polarized radiation imaging and spectroscopy mission): a white paper on the ultimate polarimetric spectro-imaging of the microwave and far-infrared sky. https://hal.archives-ouvertes.fr/hal-00838227. arXiv:1306.2259 [astro-ph.CO]